A Mechanism for Land–Atmosphere Feedback Involving Planetary Wave Structures

RANDAL D. KOSTER

Global Modeling and Assimilation Office, NASA Goddard Space Flight Center, Greenbelt, Maryland

YEHUI CHANG

Global Modeling and Assimilation Office, NASA Goddard Space Flight Center, Greenbelt, and Goddard Earth Sciences Technology and Research, Morgan State University, Baltimore, Maryland

SIEGFRIED D. SCHUBERT

Global Modeling and Assimilation Office, NASA Goddard Space Flight Center, Greenbelt, Maryland

(Manuscript received 1 May 2014, in final form 13 August 2014)

ABSTRACT

While the ability of land surface conditions to influence the atmosphere has been demonstrated in various modeling and observational studies, the precise mechanisms by which land–atmosphere feedback occurs are still largely unknown: particularly the mechanisms that allow land moisture state in one region to affect atmospheric conditions in another. Such remote impacts are examined here in the context of atmospheric general circulation model (AGCM) simulations, leading to the identification of one potential mechanism: the phase locking and amplification of a planetary wave through the imposition of a spatial pattern of soil moisture at the land surface. This mechanism, shown here to be relevant in the AGCM, apparently also operates in nature, as suggested by supporting evidence found in reanalysis data.

1. Introduction

Numerous studies with atmospheric general circulation models (AGCMs) have demonstrated the ability of soil moisture variations to affect the overlying atmosphere (e.g., Shukla and Mintz 1982; Delworth and Manabe 1989; Koster et al. 2000b; Douville et al. 2001; Guo et al. 2012). Observations-based studies are also suggestive of such impacts (e.g., Betts and Ball 1995; Findell and Eltahir 1997; Koster et al. 2003, 2011; Taylor et al. 2011). The impacts are often discussed in the context of "land–atmosphere feedback" because the affected atmospheric variables (e.g., air temperature, precipitation) are often the ones that helped produce the soil moisture variations in the first place.

The impacts identified in the literature are generally at the local scale. A wetter than average soil might change the relative magnitudes of the surface turbulent fluxes, which in turn might induce changes in the overlying boundary layer, perhaps leading to conditions more conducive to moist convection (Betts et al. 1994) or, in certain situations, to the suppression of precipitation (Findell and Eltahir 2003). A higher evaporation rate from a wetter than average soil would also reduce surface temperature through evaporative cooling, which in turn could reduce the temperature of the overlying air (e.g., Seneviratne et al. 2010).

The ability of soil moisture, however, to have a remote impact on the atmosphere—for example, an impact on near-surface air temperatures 1000 km away—is still largely undetermined, addressed by only a handful of studies (e.g., Van den Dool et al. 2003). Taylor et al. (2011) examine mechanisms for remote impacts at the mesoscale (tens to hundreds of kilometers). At even larger scales, the mechanisms must involve changes in the large-scale circulation. How this would work is still largely unexplored.

AGCMs are natural tools to explore such remote connections, despite potential limitations associated

Corresponding author address: Randal Koster, Global Modeling and Assimilation Office, Code 610.1, NASA GSFC, Greenbelt, MD 20771.
E-mail: randal.d.koster@nasa.gov

DOI: 10.1175/JCLI-D-14-00315.1

© 2014 American Meteorological Society

with their ability to resolve key processes at all relevant scales. Here we use an AGCM to explore one particular mechanism for remote soil moisture impacts on meteorological fields, a mechanism involving the phase locking of a planetary wave over a specific soil moisture pattern. We start in section 2 with a diagnostic analysis of AGCM simulations. This analysis provides the information needed to design specialty simulations (section 3) that confirm the operation of the mechanism within the model. Supporting evidence that the mechanism operates in nature as well (i.e., evidence that it is not simply a model construct) is extracted from reanalysis data in section 4. Our study concludes in section 5 with an analysis, using supplemental AGCM simulations, of two interesting facets of the feedback mechanism.

2. Analysis of atmospheric model simulations

The modeling system utilized throughout this study is the Goddard Earth Observing System Model, version 5 (GEOS-5) system of the National Aeronautics and Space Administration (NASA) Global Modeling and Assimilation Office (GMAO). All simulations examined use only the coupled atmospheric and land model components of the system, prescribing sea surface temperatures (SSTs) from observations using Atmospheric Model Intercomparison Study (AMIP)-style (Gates 1992) protocols. The atmospheric model is described in some detail by Rienecker et al. (2008) and Molod et al. (2012), and the land surface model is the catchment model of Koster et al. (2000a).

The present section focuses on the analysis of an archived ensemble of 10 simulations covering the period 1871–2011 (Schubert et al. 2014). Monthly data from these simulations are available at a resolution of $1.25° \times 1°$, the native resolution used by the model. We focus here on monthly averages of root-zone soil moisture (WRZ), 2-m air temperature (T2M), precipitation (P), and meridional wind velocity at 250 hPa (V250) taken from the last 35 yr of each simulation. Focusing on this latter period, which still provides a full 350 yr of data for analysis, allows for more consistency with reanalysis periods (section 4) and, more importantly, reduces the impact of the long-term temperature trend on our results.

Monthly soil moisture, temperature, precipitation, and V250 values were converted to standard normal deviates, or Z scores, for processing as follows:

$$Z_{\mathrm{WRZ}}(i, j, m, n) = [\mathrm{WRZ}(i, j, m, n) - M_{\mathrm{WRZ}}(i, j, m)]/\sigma_{\mathrm{WRZ}}(i, j, m), \tag{1}$$

$$Z_{\mathrm{T2M}}(i, j, m, n) = [\mathrm{T2M}(i, j, m, n) - M_{\mathrm{T2M}}(i, j, m)]/\sigma_{\mathrm{T2M}}(i, j, m), \tag{2}$$

$$Z_{P}(i, j, m, n) = [P(i, j, m, n) - M_{P}(i, j, m)]/\sigma_{P}(i, j, m), \quad \text{and} \tag{3}$$

$$Z_{\mathrm{V250}}(i, j, m, n) = [\mathrm{V250}(i, j, m, n) - M_{\mathrm{V250}}(i, j, m)]/\sigma_{\mathrm{V250}}(i, j, m), \tag{4}$$

where i and j are the longitudinal and latitudinal indices of the grid cell, m is the month, n is the year, M is the mean of a given variable over all years, and σ is its standard deviation. This standardization is useful for indicating the significance of an anomaly, since it allows the anomaly to be considered relative to the variable's interannual variability.

Our analysis focused on identifying the April soil moisture pattern over the conterminous United States (CONUS) that is most strongly related to July temperature anomalies in the U.S. Great Plains and thus may someday (with more research) be useful for prediction. Various statistical techniques (e.g., maximum covariance analysis; von Storch and Zwiers 1999) are available for isolating potential patterns; in this first study, however, guided by our initial look at the data and guided further by a desire to simplify and thereby clarify the analysis, we searched for what is arguably the simplest 2D soil moisture pattern possible: a "dipole" of soil moisture anomalies, with a positive anomaly in one location paired with a negative anomaly in another.

The dipole search proceeded as follows: For a given pairing of grid cells (representing the dipole centers), the 350 Aprils were ranked in terms of dipole strength:

$$\begin{aligned} \text{Dipole strength} &= -D_1(n)D_2(n) \quad \text{if} \quad D_1(n) > 0 \\ &= 0 \quad \text{if} \quad D_1(n) < 0, \end{aligned} \tag{5}$$

where $D_1(n)$ is the average value of Z_{WRZ} in April of year n in the 81 grid cells centered on the first chosen dipole point (so as to consider a spatial scale of ~900 km) and $D_2(n)$ is the corresponding average for the 81 grid cells centered on the second point. The subset of simulated Aprils with dipole strengths in the top 20%

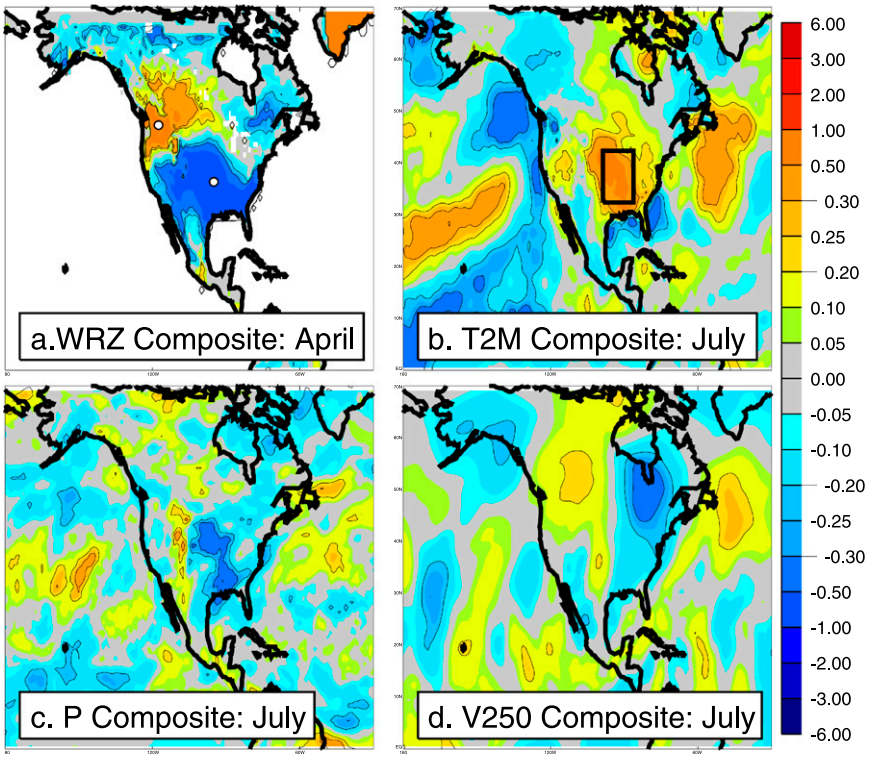

FIG. 1. (a) Composite of the standard normal deviate (Z score) of April soil moisture over the 20% of simulation years for which the April soil moisture dipole centered on the small white circles is strongest (see text). (b) Corresponding composite (i.e., for the same simulation years) of July surface air temperature Z score. (c) Corresponding composite of July precipitation Z score. (d) Corresponding composite of July 250-hPa meridional wind Z score. The contours at 0.20 and 0.30 represent values that are significantly different from zero at the 90% and 99% confidence levels, respectively.

of all values (70 Aprils in all) comprised a composite of years over which the subsequent July T2M spatial fields were averaged. This process was repeated with every possible pairing of grid cells in CONUS (indeed with both orderings of every possible pairing, so that both points in a given pairing were given the chance to represent the wet anomaly), and the particular dipole that produced the highest composited July T2M anomaly in the Great Plains was identified.

Results are shown in Fig. 1. Figure 1a shows the April Z_{WRZ} field for the composited years for the identified dipole, with the centers of this dipole marked as white circles. The associated July Z_{T2M} composite for that subset of years is shown in Fig. 1b. According to the GCM, when April soil moisture is high in the northwestern United States and low in the Great Plains, the subsequent July temperature anomaly in the Great Plains tends to be positive; the standardized anomaly corresponds to an absolute anomaly of 2 K or more in some places. Supplemental composites using different ensemble members from the same sampling of years (i.e., a random composite that would nevertheless reflect equivalent SST conditions) do not show the same signal; the July temperature signal shown is not explained by the particular SSTs of the composited years. (This is in spite of the seemingly high temperature Z scores over the oceans. The statistical significance of the oceanic T2M Z scores shown are in fact overstated, given that the 10 different ensemble members utilize the same SST forcing; over the ocean, the number of independent values making up the composite is much smaller than it is over the land.)

Figure 1c shows the average July precipitation Z scores for the composited years. A significant precipitation deficit is seen in the Great Plains, consistent with the warmer temperatures there. In absolute terms, the monthly average precipitation deficits in some places exceed 0.5 mm day^{-1}.

The dipole pattern in Fig. 1a and its impact on Great Plains temperature and precipitation is the main finding of this part of the analysis, and yet an additional point is worth making: the composited July Z_{V250} field (Fig. 1d)

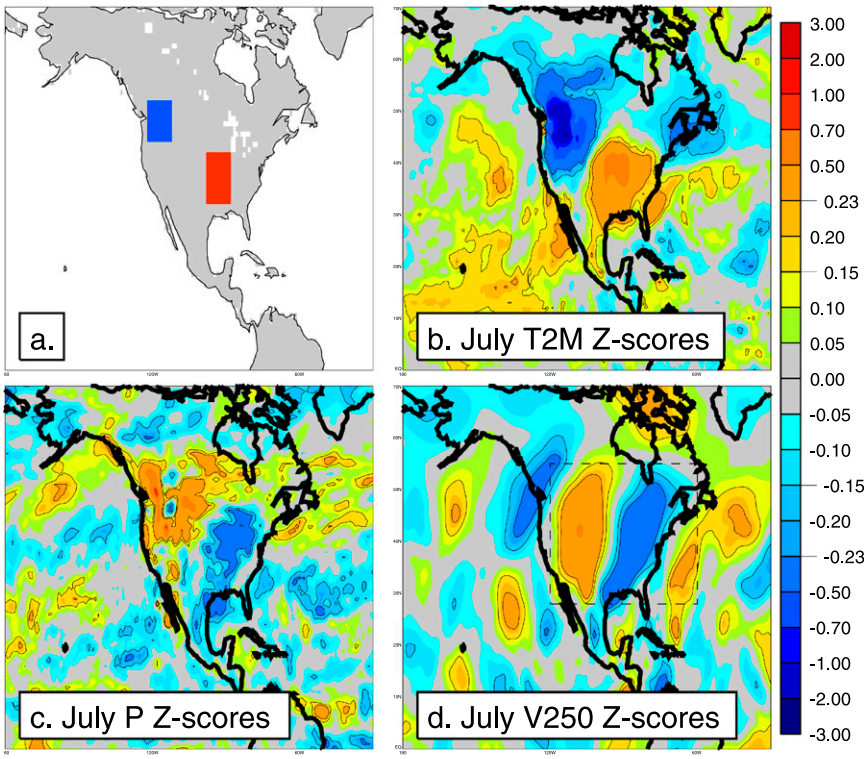

FIG. 2. (a) Locations where April precipitation is modified in a specialized experiment. April precipitation water applied to the land surface is increased fivefold in the blue area, and it is set to zero in the red area. (b) Resulting July surface air temperature anomalies, in terms of Z score (defined using moments of the control simulation). (c) Resulting July precipitation anomalies, in terms of Z score. (d) Resulting July 250-hPa meridional wind anomalies, in terms of Z score. The contours at 0.15 and 0.23 represent values that are significantly different from zero at the 90% and 99% confidence levels, respectively.

shows a distinct wave pattern, with a positive lobe of V250 anomalies in the western half of the continent and a negative lobe in the eastern half. This wave response is suggestive of an impact of land conditions on the general circulation of the atmosphere, motivating the GCM experiments discussed below.

3. Focused experiments

A hypothesis consistent with Fig. 1 is that the soil moisture pattern seen in Fig. 1a persists into the summer and, during July, affects the surface turbulent fluxes and (perhaps) precipitation in such a way as to promote the wave pattern seen in Fig. 1d, perhaps by inducing a traveling planetary wave in the troposphere to phase lock over the continent. The wave, in turn, might then exacerbate the surface Great Plains heating and drying, completing a positive feedback loop. Both segments of this loop (the land affecting the atmosphere and the atmosphere affecting the land) are now addressed in specialized AGCM experiments.

a. Experiment 1: The land–atmosphere component of the feedback loop

To examine how land conditions may affect dynamical patterns in the atmosphere, we compare two ensembles of GEOS-5 simulations covering April–July 2012, a period for which the real world experienced warm conditions in the Great Plains. The control ensemble consists of 192 AMIP-style simulations performed on a "cubed sphere" grid that generates output data on a 1° × 1° latitude–longitude grid. The simulations within the ensemble differ from each other only in their atmospheric initial conditions, taken from different years of the Modern-Era Retrospective Analysis for Research and Applications (MERRA) reanalysis (with slight perturbations imposed in each year to increase the ensemble size). The experiment ensemble is identical to the control except for the imposition of a soil moisture dipole pattern, obtained through the use of extremes in forcing: during April in these simulations, any precipitation simulated over a northwestern region of the United States (the blue box in Fig. 2a) was artificially increased fivefold

before being applied to the land surface (with the increase deposited as liquid) and precipitation simulated over the Great Plains (the red box in Fig. 2a) was zeroed. Precipitation was not modified during the May–July period.

Shown in Figs. 2b–d are the resulting differences in key July fields (experiment minus control). Here, all fields in the experiment ensemble are standardized using the means and standard deviations established in the control ensemble; shown are the averages of the resulting Z scores across the experiment ensemble. The April precipitation modifications led to soil moisture anomalies that extended into July, which in turn induced strong July temperature anomalies, including a heating in the Great Plains and a cooling in the northwestern United States (Fig. 2b). Precipitation in July was also affected (Fig. 2c), with strong deficits generated in the Great Plains and a surfeit of precipitation produced in the northwestern United States. As with the temperature changes, many of the precipitation changes in these regions are significantly different from zero at the 99% level.

The imposed soil moisture dipole had an impact on the atmosphere's general circulation as well, as manifested in the V250 winds: Fig. 2d shows a wavelike pattern in the Z_{V250} field, similar to that seen in Fig. 1d. (The anomaly correlation coefficient between the Z_{V250} fields in Figs. 1d and 2d, computed over the area within the dashed rectangle, is 0.61; higher or lower correlations can be obtained by modifying the calculation boundaries. Similarity here is mostly judged by the presence of a positive V250 lobe in the western half of the continent and a negative lobe in the eastern half, along with another positive lobe off the coast in the Atlantic.) The source of the V250 pattern can only be the imposed dipole, as all other aspects of the two ensembles are identical. The wavelike pattern does not appear until June (not shown) and July, which is consistent with the idea that soil moisture fields influence the atmosphere the most during the months of strongest insolation, when evaporation is highest.

b. *Experiment 2: The atmosphere–land component of the feedback loop*

The other phase of the feedback loop (i.e., the ability of a specific wavelike structure to induce surface warming in the Great Plains) is examined here with two additional sets of ensembles. The control for this comparison is an AMIP-style 32-member ensemble covering the period 21 May–31 July 2012. The experiment is a 32-member ensemble differing from the control in only one way: upstream of North America, within the box outlined in Fig. 3a, atmospheric conditions were forced to agree with conditions captured by the MERRA reanalysis (Rienecker et al. 2011) for the period, using a technique called "replay." The replay technique is made possible by the nature of the GEOS-5 data assimilation system, which inserts analysis increments gradually during an assimilation cycle, typically over a 6-h interval (Bloom et al. 1996). In replay mode, the analysis increments are computed from an existing analysis (in this case MERRA) to guide the evolution of model state in an (otherwise) free-running AGCM toward that of the analysis: that is, the states in the free-running AGCM are continually adjusted so that they strongly reflect those of the real world. We use here a further generalization of the approach, in which only a certain region of the atmosphere is constrained to agree with the analysis.

The motivation for this modification is the known existence of a Rossby wave pattern over North America during the hot summer of 2012 (Wang et al. 2014) and the expectation that the wave was instigated by conditions somewhere in this upstream area (e.g., Schubert et al. 2011). The hope was that, with these upstream conditions prescribed, V250 wave patterns similar to those seen in Figs. 1d and 2d would be more prevalent in the experiment ensemble than in the control ensemble. This turns out to be the case, especially in June. [The V250 patterns generated in July (not shown) are not as strong and are thus not considered further here; again, the point of this experiment is to see how a particular induced pattern affects the land variables, regardless of the particular summer month for which it occurs.] Figure 3d shows the average June Z_{V250} fields from the experiment ensemble, with the standardization performed using moments obtained from the control. A clear wavelike pattern is seen, with a positive lobe in the west and a negative lobe in the east, though with a somewhat different tilt than that seen in Figs. 1d and 2d: devising an experiment that produced a more similar pattern would require a substantial amount of trial and error. Note that, in this experiment, surface warming appears in the central United States (Fig. 3b), and precipitation is largely reduced there. The changes seen are strongly significant, perhaps partly because the imposition of upstream atmospheric conditions in the experiment ensemble leads to reduced intraensemble noise.

Given the experimental design, the changes in temperature and precipitation are a direct consequence of the upstream forcing, presumably through the generation of planetary waves; the warming appears roughly between the positive and negative lobes of the Z_{V250} field: that is, at the location of an increase in the upper-level high, where (i) subsidence tends to induce cloudless skies and thus increased surface radiative forcing

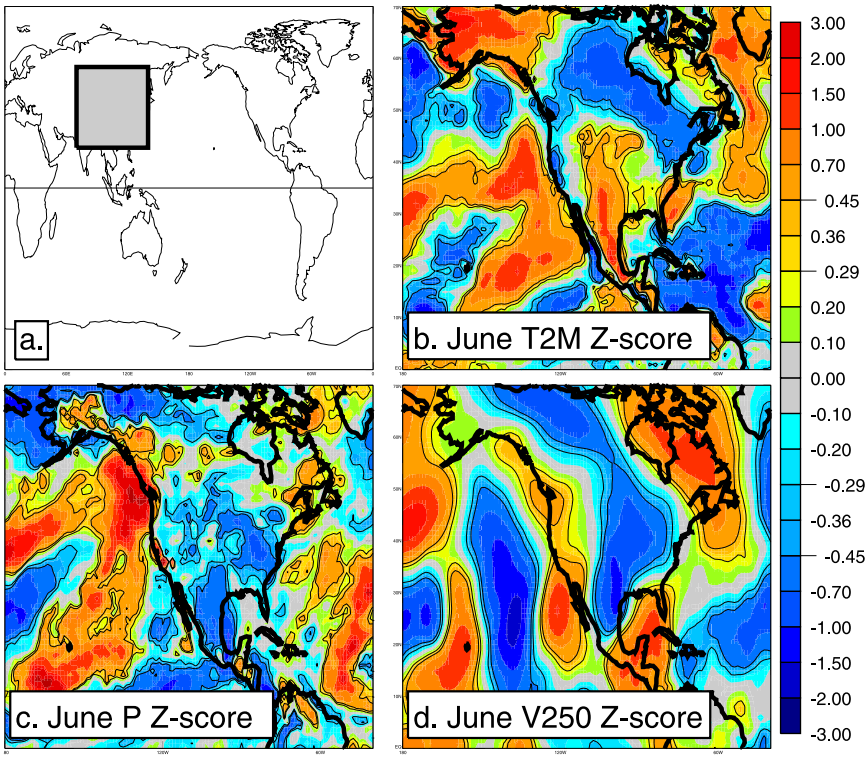

FIG. 3. (a) Location of the upstream area over which atmospheric states were forced to agree with states from an analysis (and thus were forced to be realistic), using a technique known as replay. (b) Resulting June surface air temperature anomalies. (c) Resulting June precipitation anomalies. (d) Resulting June 250-hPa meridional wind anomalies. All data represent averages over an ensemble of Z scores, defined using moments from the control simulation. The contours at 0.29 and 0.45 represent values that are significantly different from zero at the 90% and 99% confidence levels, respectively.

and (ii) surface winds tend to advect warm air in from the south. Schubert et al. (2011) found that, at monthly time scales, such waves are indeed well correlated with continental surface temperatures during summer, with correlation patterns that are consistent with the waves' largely barotropic structure, with a slight westward tilt with height. Any enhanced subsidence would also tend to reduce precipitation.

4. Supporting evidence from reanalysis

It is natural to ask if this mechanism—a soil moisture dipole inducing a planetary wave pattern, which can in turn amplify Great Plains warming—also operates in nature. Because nature does not allow the type of experiments performed in sections 2 and 3, demonstrating this conclusively is essentially impossible. Supporting evidence for the feedback is nevertheless found in the best reconstructions of historical weather available to us.

The computations underlying Fig. 4 parallel those of Fig. 1, except that, instead of producing composites from multiple centuries of simulation data, we produce them here from a 35-yr observations-based record (1979–2013). As in Fig. 1, composites are based on the strength of the soil moisture dipole in April, with a positive dipole defined as anomalously wet conditions in the northwestern United States and dry conditions in the Great Plains. Observations-based root-zone soil moistures are taken here from the North American Land Data Assimilation System (NLDAS) product (Xia et al. 2012) as produced by the variable infiltration capacity (VIC) land surface model (Liang et al. 1994). The NLDAS product is, in essence, a set of soil moistures obtained by driving a state-of-the-art land surface model with gridded observations-based meteorological forcing over the 35-yr period. Note that corresponding direct observations of root-zone soil moisture in these areas simply do not exist; gridded land data assimilation system products like these are generally considered the best estimates available for soil moisture and its year-to-year variability.

Analysis of the 35-yr NLDAS dataset identifies nine years as having a positive soil moisture dipole in April: 1981, 1982, 1986, 1996, 2000, 2003, 2006, 2011, and 2012. The composite of April soil moisture conditions over all

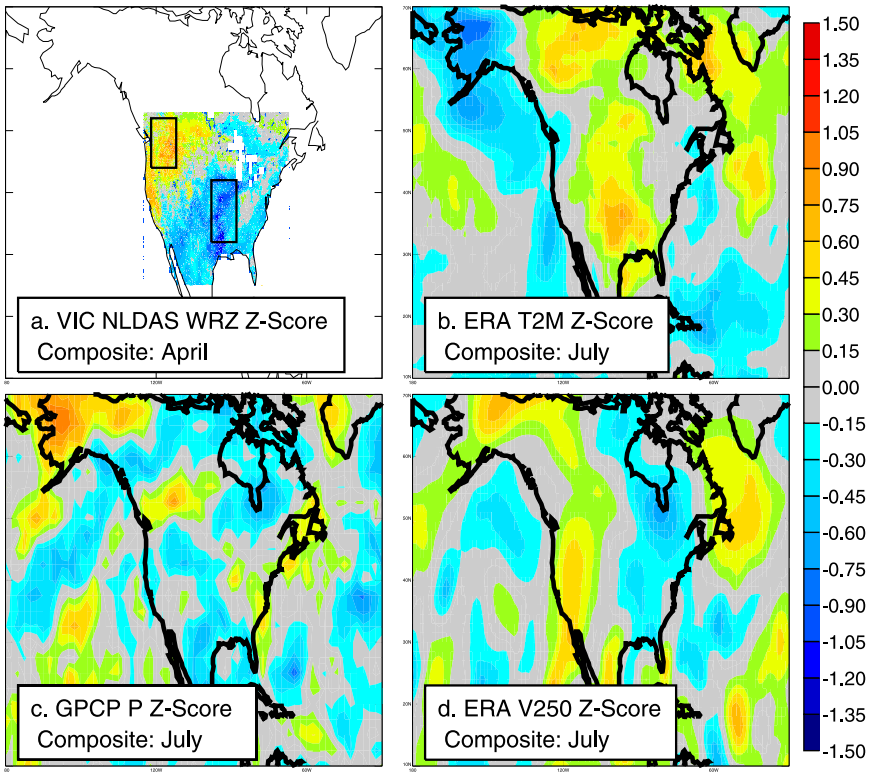

FIG. 4. (a) Composite of NLDAS-based April soil moisture, composited over the nine years for which a positive April soil moisture dipole appears in the outlined areas (see text for details). (b) Corresponding composite (i.e., for the same nine years) of July surface air temperature anomalies from the ERA-Interim dataset. (c) Corresponding composite of July precipitation anomalies from the GPCP dataset. (d) Corresponding composite of July 250-hPa meridional wind anomalies from the ERA-Interim dataset. All data are expressed in terms of Z score.

nine years (to maximize the composite size) is shown in Fig. 4a. Results are expressed in terms of average Z score, with means and standard deviations taken from the 35 yr of NLDAS data. The dipole is, by construct, apparent in the plot.

The observations-based T2M and V250 fields examined here are taken from the Interim European Centre for Medium-Range Weather Forecasts (ECMWF) Re-Analysis (ECMWF; Dee et al. 2011). The ERA-Interim T2M values are known to capture well the near-surface air temperatures measured at synoptic measurement stations (Simmons et al. 2010), presumably because the synoptic T2M measurements are themselves used to guide the ERA-Interim soil temperatures, which in turn help guide the evolution of the temperatures in the overlying air. The reanalysis V250 fields represent the best estimates available for the actual V250 values experienced in nature. While reanalysis data are not pure observations, given that model machinery is reflected to some extent in the data, the number of observations assimilated into the reanalysis over North America gives us confidence that the July T2M and V250 fields used here are realistic, reflecting what actually happened.

Reanalysis-based precipitation fields, on the other hand, are less trustworthy. The precipitation data examined here are taken from the Global Precipitation Climatology Project (GPCP) dataset, version 2.2 (Adler et al. 2003; Huffman et al. 2009; ftp://precip.gsfc.nasa.gov/pub/gpcp-v2.2/doc/), a well-regarded dataset constructed from extensive in situ gauge and satellite-based precipitation measurements.

We convert the observations-based T2M, P, and V250 data into Z scores, using means and standard deviations from the corresponding raw data fields. We then composite the data for July over the nine years used for the composite in Fig. 4a. Figure 4b shows the July Z_{T2M} composite. Warm July conditions, with an average anomaly of up to 1 K or more (in terms of absolute anomaly), are found in the Great Plains for the subsetted years: the historical temperature anomalies were arguably predictable from the presence of the April soil moisture dipole. The composited years also show

a deficit of precipitation in the Great Plains (Fig. 4c), with some local deficits approaching 1 mm day^{-1}. Furthermore, the composite July Z_{V250} anomaly field for these years (Fig. 4d) shows a pattern very similar to that seen in Figs. 1d and 2d (with a spatial anomaly correlation coefficient of 0.60 relative to Fig. 1d, over the rectangular area outlined in Fig. 2d), supporting the idea that the soil moisture dipole had an impact on the planetary wave structure.

These results cannot be considered conclusive; indeed, given the small size of the composite, the values plotted in Figs. 4b,c are generally not statistically significant. Individual years might not show the indicated patterns. Nevertheless, the patterns in the composited data are fully consistent with the feedback mechanism established for the AGCM. The agreement between the patterns shown in Fig. 4 with those of the earlier figures either constitutes support for the feedback mechanism or must be deemed a strong coincidence.

ERA-Interim was used for Fig. 4 because its T2M product is tied strongly to synoptic air temperature measurements, lending credence to its near-surface temperature product. The MERRA reanalysis (Rienecker et al. 2011) produced by the Global Modeling and Assimilation Office of the NASA Goddard Space Flight Center does not similarly ingest these near-surface synoptic measurements; even so, processing the T2M (and V250) fields from MERRA produces composite fields (not shown) that are almost identical to those in Figs. 4b,d. The results in Figs. 4b,d thus appear robust with respect to the reanalysis considered.

5. Discussion

The findings above regarding the soil moisture dipole (wet conditions in the northwestern United States and dry conditions in the Great Plains) and its effects on temperature, precipitation, and 250-hPa winds raises a number of additional interesting questions. We address two of these questions here.

a. How does the impact of the soil moisture dipole compare with that of a soil moisture monopole?

The targeted soil moisture pattern sought in section 2 and thereafter examined with our AGCM experiments was a simple dipole: dry conditions in one location and wet conditions in another. Searching instead for a soil moisture monopole (not shown), arguably the simplest pattern of all, locates the optimal monopole in the Great Plains itself, with dry Great Plains soil moisture conditions tending to lead to warm summer Great Plains temperatures. The monopole search thus appears to address local land–atmosphere feedback, wherein dry April soil moistures are remembered into July, leading to reduced evaporative cooling during that month. The dipole search, in contrast, is found to be more conducive to examining mechanisms underlying remote impacts. This said, it is still worth examining the impacts of monopole soil moisture anomalies on subsequent temperatures and precipitation rates (local and remote) and on the large-scale circulation.

We address this here with an extension of experiment 1 of section 3a. Recall that, in that experiment, manipulation of the AGCM's precipitation during April produced an anomalously dry springtime soil moisture state in the Great Plains and a wet state in the northwestern United States; the experiment went on to examine the consequent impacts of these conditions on T2M, P, and V250 fields in July. Here, we supplement that analysis with two additional ensembles: a 192-member ensemble in which only the April precipitation modifications over the northwestern United States are applied and a 192-member ensemble in which only those modifications over the Great Plains are applied. In other words, the first supplemental ensemble imposes a wet monopole of springtime soil moisture in the northwestern United States, whereas the second imposes a springtime dry monopole in the Great Plains.

Results are shown in Fig. 5. Figures 5a,e,i,m show the locations of the imposed springtime anomalies, and the other panels show the resulting changes in July T2M (Figs. 5b,f,j,n), P (Figs. 5c,g,k,o), and V250 (Figs. 5d,h,l,p) Z scores.

Figures 5a–d show that imposing wet conditions during spring in the northwestern United States leads to cool July temperatures and high precipitation anomalies in this area (Figs. 5b,c). Notice, however, that it also leads to a significant warm anomaly in the southern Great Plains, along with significant precipitation deficits there. These remote impacts are indeed consistent with the induced wavelike structure of the July V250 anomalies seen in Fig. 5d. The monopole structure, by itself, has an impact on the general circulation (along the lines of that seen in Fig. 2d) and on remote surface air temperatures and precipitation rates.

Figures 5b–d thus provide the clearest indication yet that a mechanism for remote land–atmosphere feedback does operate in the model. In contrast, Figs. 5f,g show that, while an imposed Great Plains dry anomaly induces warm July surface air temperatures in the Great Plains (presumably through local feedback), it does not greatly affect remote temperatures or precipitation rates. The dry Great Plains anomaly is accordingly seen to have a small, though still significant, impact on the V250 field (Fig. 5h), weaker than that seen for the wet northwestern U.S. anomaly.

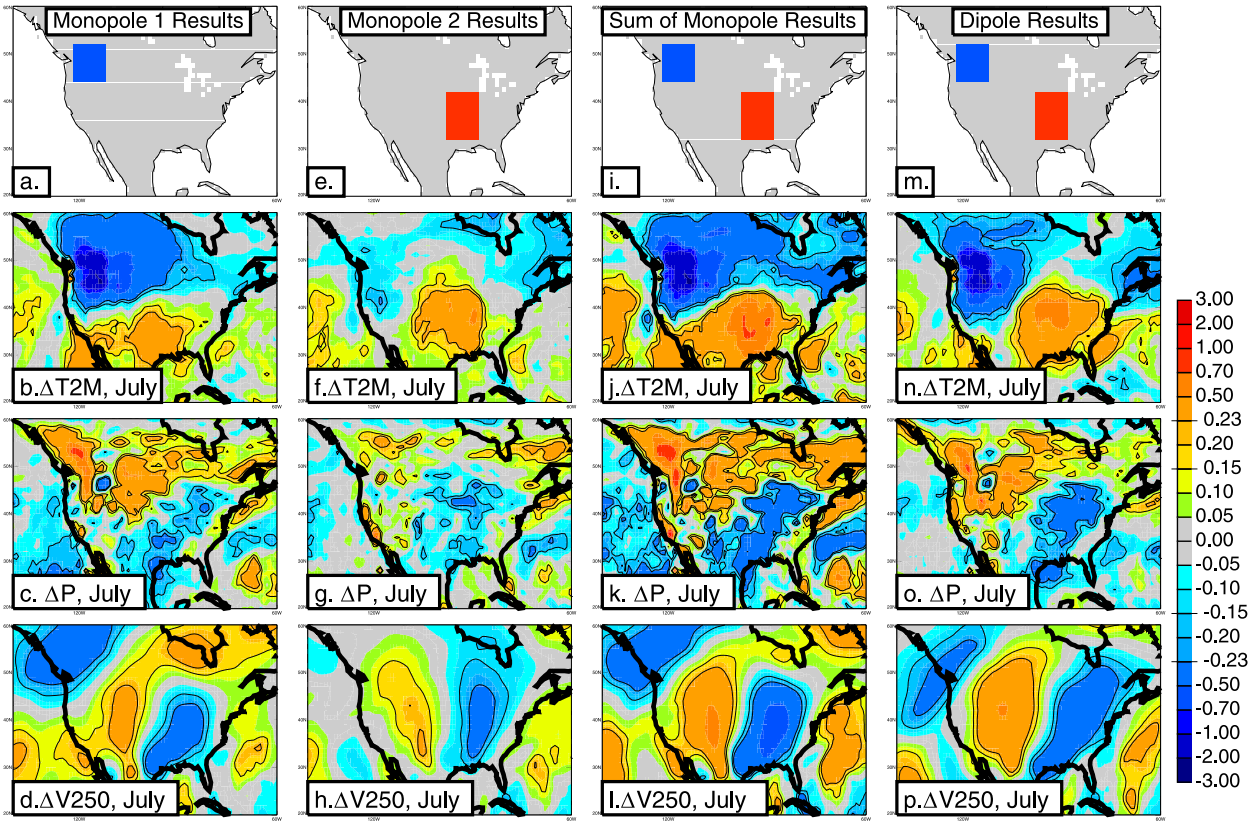

FIG. 5. As in Fig. 2, but for supplemental experiments. (a),(e),(i),(m) The locations of the imposed April anomalies (blue for wet and red for dry); (b),(f),(j),(n) the resulting ensemble average Z score of July surface air temperature; (c),(g),(k),(o) the resulting ensemble average Z score of July precipitation; and (d),(h),(l),(p) the corresponding ensemble average Z score of July V250 winds. (a)–(d) Results for the ensemble in which a wet anomaly (a wet monopole) is applied in the northwestern United States. (e)–(h) Results for the ensemble in which a dry anomaly (a dry monopole) is applied in the Great Plains. (i)–(l) Sum of the results from (a)–(h). (m)–(p) The dipole ensemble results, repeated from Fig. 2. The contours at 0.15 and 0.23 represent values that are significantly different from zero at the 90% and 99% confidence levels, respectively.

The sum of the anomaly fields from the two monopole ensembles is shown in Figs 5i–l; this sum can be directly compared to the dipole ensemble results of Fig. 2, which are repeated in Figs. 5m–p. Notice that corresponding plots in Figs. 5i–p are quite similar in terms of the positions and magnitudes of the anomalies. The agreement implies two things: 1) the AGCM experiment results are robust (i.e., the first-order signals seen in the plots are not random) and 2) the monopole results contribute independently and linearly to the results obtained with the imposed dipole. It appears that, to first order, results for the dipole are strong because of these independent contributions: each contribution helps to phase lock the planetary wave in the position needed to enhance Great Plains warming.

b. *Does the land surface act mainly to strengthen an SST-induced atmospheric signal?*

The experiment in section 3a shows how the model's atmosphere responds to an imposed dipole of soil moisture anomalies. Not addressed by that experiment, however, is whether the imposed dipole can produce this atmospheric response by itself. It is quite possible that the SST conditions in 2012, the year examined, promoted the particular V250 pattern seen in Fig. 2d and that the imposed soil moisture anomalies acted only to amplify the preexisting pattern.

We examine this possibility with two additional ensembles performed in the manner of the experiment in section 3a. The first new ensemble imposes the dipole pattern of soil moisture anomalies seen in Fig. 2a, with a positive anomaly in the northwestern United States and a negative anomaly in the Great Plains, whereas the second imposes the reverse pattern, with dry conditions in the northwestern United States and wet conditions in the Great Plains. The two new ensembles are otherwise identical to that described in section 3a, except for the period over which the anomalies are imposed: in these two new ensembles, both the artificial zeroing of the

precipitation in the selected dry area and the artificial amplification of the precipitation in the selected wet area are maintained throughout the 4-month simulation period rather than only in April. The dipoles are artificially maintained in this way because our goal in this section is to demonstrate that different soil moisture patterns can lead to different atmospheric responses regardless of the background SST state. In other words, implications for prediction are not provided here. Indeed, when the reverse dipole (dry northeastern United States and wet Great Plains) is imposed only in April (results not shown), the July V250 fields do not show much of a signal; in contrast to the system memory associated with the original dipole, that associated with the reverse dipole is apparently not large enough to support the planetary wave feedback mechanism at the interseasonal time scale.

Figures 6a–d show the results for the ensemble with the original dipole (maintained throughout the period), and Figs. 6e–h show the corresponding results for the reverse dipole. The continental temperature responses in July (Figs. 6e,f; the temperature anomalies are shown as Z scores, constructed using moments from the control experiment in section 3a) are to a large extent mirror images of each other: the original dipole produces the pattern already seen in Fig. 2b, though with stronger magnitudes because of the stronger July soil moisture anomalies, and the reverse dipole produces the corresponding reverse result (Fig. 6f), with warm temperatures in the northwestern United States and cool temperatures in the Great Plains. The precipitation responses are also reversed, especially over the Great Plains area, where dry and wet soil moisture anomalies produce precipitation deficits and surfeits, respectively.

Most of these differences almost certainly result from local effects: for example, from the influence of soil moisture on local evaporative cooling and from the impact of soil moisture on the local generation of precipitation. Even so, the V250 wind field patterns (shown in Figs. 6d,h) are also reversed in the second ensemble, both over the continent and downwind of the continent, over the northern Atlantic. The two opposite soil moisture patterns thus induce correspondingly reversed planetary wave patterns. The V250 pattern produced in each ensemble is amenable to the further amplification of that ensemble's particular surface air temperature and precipitation anomaly patterns through the mechanisms discussed in section 3b.

The background SST field would at most support only one of the two V250 patterns shown in Figs. 6d,h. The contrast in Figs. 6d,h thus demonstrates that, at least in the model, soil moisture anomalies can induce a planetary wave response all by themselves, without the benefit of a background SST field. This said, it is worth noting that the magnitudes of the V250 Z scores are larger for the original dipole structure. This may indeed be due to the particular set of SSTs used in the experiment (those for 2012); more analysis would be needed to pin this down.

6. Summary

Figure 2 shows that, in the AGCM, imposing a dipole structure in April soil moisture, with wet conditions in the northwestern United States and dry conditions in the Great Plains, promotes a July wave pattern in the atmosphere. Figure 3 shows that instigating such a wave pattern (in this case through a remote mechanism, over Asia) leads to increased 2m air temperatures and reduced precipitation in the U.S. Great Plains and, to a small extent, cooler temperatures over the northwestern United States, bolstering the surface temperature signal. Considered together, the two figures describe a continental-scale land–atmosphere feedback mechanism. While much of the Great Plains temperature anomaly in Fig. 2b is presumably a reflection of drier soil moistures there and the associated decrease in evaporative cooling and while much of the precipitation anomaly presumably reflects local impacts of soil moisture on precipitation formation, not all of the impacts are local. The induced formation of the wave structure and its ability to feed back on the temperature and precipitation anomaly fields constitutes a positive feedback loop for the model climate, one involving a change in the large-scale circulation and, accordingly, an impact of soil moisture anomalies on near-surface air temperature and precipitation in remote locations. This is made very clear in the supplemental experiments utilizing monopoles of soil moisture anomalies. Figures 5b–d show that imposing a wet monopole of April soil moisture in the northwestern United States induces a wavelike structure in the V250 winds and consistent changes in temperature and precipitation as far away as the Great Plains.

Does this mechanism also operate in nature? Supporting evidence for the mechanism is seen in observational data (Fig. 4); a composite of observed fields over the nine years in the period 1979–2013 that have a soil moisture dipole in April shows patterns consistent with those seen in the AGCM experiments. A sample size of nine, however, is much too small to provide adequate statistical proof, especially because the dipole only implies an increased probability of the indicated July response, not a guarantee. The observational analysis can be only said to support the model results; it cannot be said to validate them.

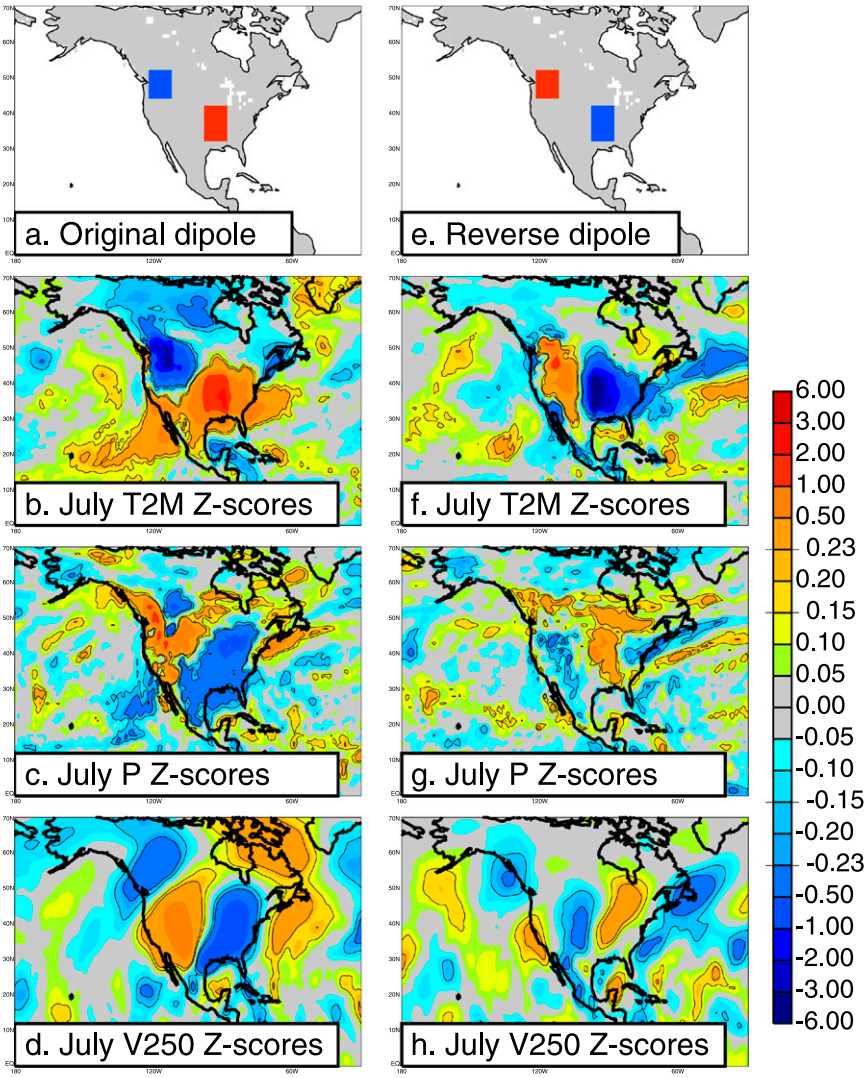

FIG. 6. (a) Pattern of soil moisture anomalies imposed over a 4-month period in an ensemble of AGCM simulations: wet conditions in the northwestern United States and dry conditions in the Great Plains. (b) Corresponding ensemble mean Z scores (standardized with statistics from the control in section 3a) for July surface air temperature. (c) Corresponding ensemble mean Z scores for precipitation. (d) Corresponding ensemble mean Z scores for July V250 winds. (e)–(g) As in (a)–(d), but for the reversed pattern of soil moisture anomalies, with dry conditions in the northwestern United States and wet conditions in the Great Plains. The contours at 0.15 and 0.23 represent values that are significantly different from zero at the 90% and 99% confidence levels, respectively.

The dipole identified and utilized in our experiments is, of course, only one of potentially many soil moisture patterns of relevance to continental-scale land–atmosphere feedback mechanisms in the climate system. The approaches presented here could prove useful in identifying and analyzing additional patterns.

Acknowledgments. Support for this project was provided by the NOAA Modeling, Analysis, Predictions and Projections (MAPP) program; the NASA Energy and Water Cycle Study (NEWS) program; and the NASA Modeling, Analysis, and Prediction Program. We thank Sarith Mahanama, Greg Walker, and Hailan Wang for help with dataset logistics.

REFERENCES

Adler, R. F., and Coauthors, 2003: The Version-2 Global Precipitation Climatology Project (GPCP) monthly precipitation

analysis (1979–present). *J. Hydrometeor.,* **4,** 1147–1167, doi:10.1175/1525-7541(2003)004<1147:TVGPCP>2.0.CO;2.

Betts, A. K., and J. H. Ball, 1995: The FIFE surface diurnal cycle climate. *J. Geophys. Res.,* **100,** 25 679–25 693, doi:10.1029/94JD03121.

——, ——, A. C. M. Beljaars, M. J. Miller, and P. Viterbo, 1994: Coupling between land-surface, boundary-layer parameterizations and rainfall on local and regional scales: Lessons from the wet summer of 1993. *Proc. Fifth Conf. on Global Change Studies,* Nashville, TN, Amer. Meteor. Soc., 174–181.

Bloom, S., L. Takacs, A. DaSilva, and D. Ledvina, 1996: Data assimilation using incremental analysis updates. *Mon. Wea. Rev.,* **124,** 1256–1271, doi:10.1175/1520-0493(1996)124<1256:DAUIAU>2.0.CO;2.

Dee, D. P., and Coauthors, 2011: The ERA-Interim reanalysis: Configuration and performance of the data assimilation system. *Quart. J. Roy. Meteor. Soc.,* **137,** 553–597, doi:10.1002/qj.828.

Delworth, T. L., and S. Manabe, 1989: The influence of soil wetness on near-surface atmospheric variability. *J. Climate,* **2,** 1447–1462, doi:10.1175/1520-0442(1989)002<1447:TIOSWO>2.0.CO;2.

Douville, H., F. Chauvin, and H. Broqua, 2001: Influence of soil moisture on the Asian and African monsoons. Part I: Mean monsoon and daily precipitation. *J. Climate,* **14,** 2381–2403, doi:10.1175/1520-0442(2001)014<2381:IOSMOT>2.0.CO;2.

Findell, K. L., and E. A. B. Eltahir, 1997: An analysis of the soil moisture-rainfall feedback, based on direct observations from Illinois. *Water Resour. Res.,* **33,** 725–735, doi:10.1029/96WR03756.

——, and ——, 2003: Atmospheric controls on soil moisture-boundary layer interactions. Part I: Framework development. *J. Hydrometeor.,* **4,** 552–569, doi:10.1175/1525-7541(2003)004<0552:ACOSML>2.0.CO;2.

Gates, W. L., 1992: AMIP: The Atmospheric Model Intercomparison Project. *Bull. Amer. Meteor. Soc.,* **73,** 1962–1970, doi:10.1175/1520-0477(1992)073<1962:ATAMIP>2.0.CO;2.

Guo, Z. C., P. A. Dirmeyer, T. DelSole, and R. D. Koster, 2012: Rebound in atmospheric predictability and the role of the land surface. *J. Climate,* **25,** 4744–4749, doi:10.1175/JCLI-D-11-00651.1.

Huffman, G. J., R. F. Adler, D. T. Bolvin, and G. Gu, 2009: Improving the global precipitation record: GPCP version 2.1. *Geophys. Res. Lett.,* **36,** L17808, doi:10.1029/2009GL040000.

Koster, R. D., M. J. Suarez, A. Ducharne, M. Stieglitz, and P. Kumar, 2000a: A catchment-based approach to modeling land surface processes in a general circulation model: 1. Model structure. *J. Geophys. Res.,* **105,** 24 809–24 822, doi:10.1029/2000JD900327.

——, ——, and M. Heiser, 2000b: Variance and predictability of precipitation at seasonal-to-interannual timescales. *J. Hydrometeor.,* **1,** 26–46, doi:10.1175/1525-7541(2000)001<0026:VAPOPA>2.0.CO;2.

——, ——, R. W. Higgins, and H. M. Van den Dool, 2003: Observational evidence that soil moisture variations affect precipitation. *Geophys. Res. Lett.,* **30,** 1241, doi:10.1029/2002GL016571.

——, and Coauthors, 2011: The second phase of the Global Land–Atmosphere Coupling Experiment: Soil moisture contributions to subseasonal forecast skill. *J. Hydrometeor.,* **12,** 805–822, doi:10.1175/2011JHM1365.1.

Liang, X., D. P. Lettenmaier, E. F. Wood, and S. J. Burges, 1994: A simple hydrologically based model of land surface water and energy fluxes for general circulation models. *J. Geophys. Res.,* **99,** 14 415–14 428, doi:10.1029/94JD00483.

Molod, A., L. Takacs, M. Suarez, J. Bacmeister, I.-S. Song, and A. Eichmann, 2012: The GEOS-5 atmospheric general circulation model: Mean climate and development from MERRA to Fortuna. Technical Report Series on Global Modeling and Data Assimilation, NASA Tech. Memo. NASA/TM-2012-104606, Vol. 28, 124 pp.

Rienecker, M. M., and Coauthors, 2008: The GEOS-5 data assimilation system—Documentation of versions 5.0.1, 5.1.0, and 5.2.0. Technical Report Series on Global Modeling and Data Assimilation, NASA Tech. Memo. NASA/TM-2008-104606, Vol. 27, 118 pp.

——, and Coauthors, 2011: MERRA: NASA's Modern-Era Retrospective Analysis for Research and Applications. *J. Climate,* **24,** 3624–3648, doi:10.1175/JCLI-D-11-00015.1.

Schubert, S., H. Wang, and M. Suarez, 2011: Warm season subseasonal variability and climate extremes in the Northern Hemisphere: The role of stationary Rossby waves. *J. Climate,* **24,** 4773–4792, doi:10.1175/JCLI-D-10-05035.1.

——, ——, R. Koster, M. Suarez, and P. Groisman, 2014: Northern Eurasian heat waves and droughts. *J. Climate,* **27,** 3169–3207, doi:10.1175/JCLI-D-13-00360.1.

Seneviratne, S. I., T. Corti, E. L. Davin, M. Hirschi, E. B. Jaeger, I. Lehner, B. Orlowsky, and A. J. Teuling, 2010: Investigating soil moisture–climate interactions in a changing climate: A review. *Earth-Sci. Rev.,* **99,** 125–161, doi:10.1016/j.earscirev.2010.02.004.

Shukla, J., and Y. Mintz, 1982: Influence of land-surface evapotranspiration on the earth's climate. *Science,* **215,** 1498–1501, doi:10.1126/science.215.4539.1498.

Simmons, A. J., K. M. Willett, P. D. Jones, P. W. Thorne, and D. P. Dee, 2010: Low-frequency variations in surface atmospheric humidity, temperature, and precipitation: Inferences from reanalyses and monthly gridded observational data sets. *J. Geophys. Res.,* **115,** D01110, doi:10.1029/2009JD012442.

Taylor, C. M., A. Gounou, F. Guichard, P. P. Harris, R. J. Ellis, F. Couvreux, and M. De Kauwe, 2011: Frequency of Sahelian storm initiation enhanced over mesoscale soil-moisture patterns. *Nat. Geosci.,* **4,** 430–433, doi:10.1038/ngeo1173.

Van den Dool, H., J. Huang, and Y. Fan, 2003: Performance and analysis of the constructed analogue method applied to U.S. soil moisture over 1981-2001. *J. Geophys. Res.,* **108,** 8617, doi:10.1029/2002JD003114.

von Storch, H., and F. W. Zwiers, 1999: *Statistical Analysis in Climate Research*. Cambridge University Press, 484 pp.

Wang, H., S. Schubert, R. Koster, Y.-G. Ham, and M. Suarez, 2014: On the role of SST forcing in the 2011 and 2012 extreme U.S. heat and drought: A study in contrasts. *J. Hydrometeor.,* **15,** 1255–1273, doi:10.1175/JHM-D-13-069.1.

Xia, Y., and Coauthors, 2012: Continental-scale water and energy flux analysis and validation for the North American Land Data Assimilation System project phase 2 (NLDAS-2): 1. Intercomparison and application of model products. *J. Geophys. Res.,* **117,** D03109, doi:10.1029/2011JD016048.